

# Journal of Mechanics of Materials and Structures

**FAILURE PATTERN PREDICTION IN MASONRY**

Gianmarco De Felice and Marialaura Malena

Volume 14, No. 5

December 2019



## FAILURE PATTERN PREDICTION IN MASONRY

GIANMARCO DE FELICE AND MARIALAURA MALENA

The structural assessment of masonry remains an open challenge due to its intrinsic nonhomogenous nonisotropic and nonlinear behavior. Aiming at providing a tool for structural applications, this paper presents the formulation and implementation in a FE code of a simple constitutive model to describe the behavior of masonry walls regarded as elastoplastic homogenized anisotropic plates. The model is based on few geometrical and mechanical parameters that can be easily detected from masonry typology. Nonetheless, it can capture the essential features of the structural behavior of ancient masonry, i.e., the failure in traction and the anisotropic behavior deriving from the joints layout. The model succeeded in predicting the failure mechanism and load carrying capacity under different boundary and loading conditions, including soil settlement and seismic loading. Its validation is finally carried out for some selected case studies.

### 1. Introduction

The response of ancient masonry structures under foundation settlements or seismic events is usually affected by local failure modes which typically involve both in-plane and out-of-plane collapse mechanisms. The prediction of the failure patterns associated with these mechanisms can be carried out using different analysis and modelling approaches [de Felice et al. 2017]. When numerical analysis is adopted, an adequate constitutive law for the masonry is requested. Considering the uncertainties that typically affect the detection of the structural properties of historical constructions, numerical models suitable for analyses should be as simple as possible and based on few mechanical parameters. In the meantime, the model should be able to describe some essential features of masonry behavior, such as: the ability to capture the failure in traction, the inclusion of the anisotropic behavior, at least in terms of failure condition, and the capability to reproduce the failure pattern under different boundary and loading conditions.

A considerable number of nonlinear models have been developed for masonry, aiming at capturing the essential no-tensile strength under traction [Angelillo 1993; Angelillo et al. 2010], according to the well-known Heyman hypothesis [Heyman 1966], or the complex interaction between masonry units, resulting in an overall anisotropic behavior [Page 1978; de Buhan and de Felice 1997; Sacco 2009; Zucchini and Lourenço 2002; Massart et al. 2005; Sab 2003; Stefanou et al. 2015; Amorosi et al. 2012; 2014; Roselli et al. 2018]. More complex three-dimensional models have been proposed in the framework of either continuum [Milani et al. 2006a; 2007], or discrete limit analysis [Livesley 1978; Portioli et al. 2014], or resorting to a discrete macroelements approach [Calió et al. 2012].

---

*Keywords:* masonry, FE model, failure pattern, plastic strain, settlement, earthquake loads.

In this work, an elastic perfectly-plastic plate model able to describe the nonlinear behavior of masonry walls subject to both in-plane and out-of-plane loads is proposed. The model is an extension of a previous formulation in which only the in-plane behavior was considered [de Felice et al. 2010].

The proposed model represents the masonry wall as an elastoplastic homogenized Love–Kirchhoff plate, with associated flow-rule. The macroscopic elastic properties are obtained through a micro mechanical approach, while the strength domain is assumed to coincide with the one defined in [Sab 2003; Sab et al. 2007], derived by a homogenization procedure on a thin periodic heterogeneous plate made of 3D infinitely resistant blocks connected by Mohr–Coulomb interfaces.

In the present case, the cohesive contribution of the mortar joints is practically neglected. This hypothesis, widely used in modelling masonry after Heyman’s contribution, seems appropriate for old structures, since the joints have experienced loss of mortar or degradation of its mechanical properties, due to environmental ageing conditions. Accordingly, the old masonry structure becomes similar to a dry joints masonry structure. On the other hand, material crushing under compression is neglected as well, since masonry units are supposed having infinite compressive strength. This hypothesis, in agreement with Heyman’s assumptions, appears justified for the problems at hand (soil settlement and earthquake loads in low-rise buildings), for which material crushing does not occur since the compressive stress remains much lower than the material strength. It should be pointed out that the no-tensile and infinite compression hypotheses do not yield to the well known no-tension model since the model, according to the homogenization approach, includes a pseudo tensile strength in the horizontal direction deriving from the interlocking of masonry blocks and the presence of friction at the interfaces.

The model has been implemented in the Finite Element code Abaqus in the context of perfect plasticity theory, aiming at carrying out path-following nonlinear analyses of masonry structures under various loading and boundary conditions. If on the one hand, a path-following analysis requires a computation cost higher than the limit analysis, on the other hand, it provides the whole equilibrium path under external loads that, for instance, can be used for the seismic assessment through pushover analysis [Acito et al. 2016]. It is worth noting that, according to experimental evidences [Lourenço and Ramos 2004], material behavior of masonry constituents is not perfectly plastic, but generally exhibit a softening behavior both in compression, once crushing is attained, and in traction, once the tensile strength is reached. However, in the present case, as both, joint cohesion and crushing in compression, are neglected, there is no reason to include the softening behavior, that would induce computational problems of mesh dependence and difficulties in convergence. The hypothesis of associated plastic flow-rule does not completely reflect the behavior of masonry since, especially in presence of high compressive stresses, sliding in mortar joints occur without dilatancy. This hypothesis could represent a serious drawback for the case of masonry constructions having boundary conditions constraining the joint dilatation. Hence, in general terms, the proposed model provides only an upper bound prediction of the failure load, that should be prudently adopted. However, as usually masonry walls are simply subjected to self-weight, for current problems, the hypothesis of associated flow-rule does not significantly affect the prediction of failure load. Moreover, the hypothesis is straightforward to apply the Haar–Karman’s principle in the solution procedure.

A further drawback of the proposed model is that, since a Love–Kirchhoff plate is adopted, the shear deformation and the possible disaggregation of the wall in out-of-plane bending are neglected. Both these phenomena that may occur in thick walls, are therefore disregarded, since the model more accurately describes the behavior of thin walls. In fact, according to [Cecchi et al. 2007] there are no meaningful

differences between the Love–Kirchhoff model and the Reissner–Mindlin model when thin walls are considered.

This model has been also adopted in a previous work of Malena et al. [2019], where a comparison with the results of limit analysis of structures made of rigid blocks is presented in the way to highlight the weakness and the potentiality of continuous versus discrete formulations.

In the first section, the model is formulated in terms of elastic properties, strength conditions and elastic-plastic constitutive law. Then, in Section 2, the results of numerical simulations of masonry walls under foundation settlements are presented and compared with the outcomes of a more accurate discrete model [Malena et al. 2019; Portioli and Cascini 2016]. Finally, in Section 3, the numerical simulations of a prototype consisting of three U-shaped connected walls subjected to horizontal loads are presented and compared with experimental outcomes presented in [Restrepo Vélez et al. 2014], to assess the capability of the model to predict the failure patterns resulting from seismic action.

## 2. Masonry model

Let us consider the masonry wall in Figure 1, made of parallelepiped blocks having thickness  $h$ , height  $a$  and length  $b$ , arranged in a regular pattern and bonded with mortar joints. Mortar joints are viewed as interfaces forming a regular network of two sets of orthogonal planes: horizontal bed joints (parallel to the  $Ox_1x_3$  plane) are continuous, while vertical head joints (parallel to the  $Ox_2x_3$  plane) are discontinuous, as a result of the running bond pattern.

If the dimensions of the blocks are small when compared with the sizes of the wall  $L$ ,  $H$ , and if the actions are characterized by a wavelength much larger than the size of the blocks, according to [Caillerie 1984], the masonry wall can be represented as a homogenized continuum Love–Kirchhoff plate. In this case, the masonry wall occupies the domain  $\Omega \times ]-h/2; h/2[$  (Figure 1), where  $\Omega$  is its middle plane and  $h$  the corresponding out-of-plane thickness.

**2A. Macroscopic elastic properties.** The elastic properties of masonry may be derived from the properties of its constituents according to the homogenization theory for periodic media, through the resolution of a boundary value problem on the unit cell with periodicity conditions. By adopting reasonable simplifications on the geometry of the unit cell, a closed form solution is available. In most contributions

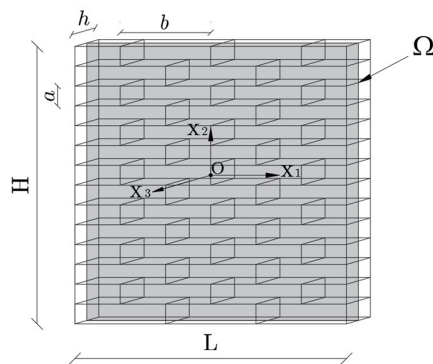


**Figure 1.** Block structure.

in the literature, only the in-plane behavior of masonry was investigated: in [de Felice 1995] the elastic macroscopic properties have been deduced under condition that the blocks behave as rigid bodies and the joints are simply interfaces that control the deformability of the assembly; in [de Felice 2001; Cecchi and Sab 2002] the contribution in deformation provided by the blocks has been accounted for, assuming a constant strain field; in [Milani et al. 2006b] an affine displacement field has been assumed in both, the blocks and the joints, taking into account the finite thickness of these latter. Whenever addressed, the out-of-plane behavior refers either to the shear deformation of masonry bulk, [Zucchini and Lourenço 2002; Pande et al. 1989; Pietruszczak and Niu 1992], or to the joint contribution to bending [Cecchi and Sab 2002; Mistler et al. 2007; Taliercio 2016].

In this work, according to [Mistler et al. 2007], the orthotropic equivalent elastic properties of masonry are based on the following macroscopic parameters: the Young’s moduli in the horizontal and vertical directions  $E_1$  and  $E_2$ , the Poisson ratios  $\nu_{12}$ ,  $\nu_{21}$  and the shear modulus  $G_{12}$ , which are based on mechanical and geometrical properties of the constituents as shown hereafter. Let us define the vector  $\mathbf{t} = (\mathbf{N}, \mathbf{M})$  collecting, for the homogenized plate, the macroscopic in-plane (membrane) forces  $\mathbf{N} = N_{\alpha\beta}$  and out-of-plane bending moments  $\mathbf{M} = M_{\alpha\beta}$ , and the vector  $\boldsymbol{\varepsilon} = (\mathbf{E}, \boldsymbol{\chi})$  collecting the corresponding in-plane strain  $\mathbf{E} = E_{\alpha\beta}$  and out-of-plane curvature  $\boldsymbol{\chi} = \chi_{\alpha\beta}$ , for  $\alpha, \beta = 1, 2$ . The flexibility matrix  $\mathbf{A}$  relating the membrane strains and curvatures to the membrane forces and bending moments is given by

$$\begin{pmatrix} E_{11} \\ E_{22} \\ 2E_{12} \\ \chi_{11} \\ \chi_{22} \\ 2\chi_{12} \end{pmatrix} = \begin{pmatrix} 1/hE_1 & -\nu_{12}/hE_1 & 0 & 0 & 0 & 0 \\ -\nu_{21}/hE_2 & 1/hE_2 & 0 & 0 & 0 & 0 \\ 0 & 0 & 1/hG_{12} & 0 & 0 & 0 \\ 0 & 0 & 0 & 12/h^3E_1 & -12\nu_{12}/h^3E_1 & 0 \\ 0 & 0 & 0 & -12\nu_{21}/h^3E_2 & 12/h^3E_2 & 0 \\ 0 & 0 & 0 & 0 & 0 & 12/h^3G_{12} \end{pmatrix} \begin{pmatrix} N_{11} \\ N_{22} \\ N_{12} \\ M_{11} \\ M_{22} \\ M_{12} \end{pmatrix}. \tag{2-1}$$

The coefficients in (2-1), as shown in the previous work [de Felice et al. 2010], depend on the elastic properties of blocks ( $\lambda'_b, \mu_b$ ) and joints ( $K_n, K_t$ ) and on the dimensions of the blocks ( $a, b$ ) as

$$\frac{1}{E_1} = \frac{4a}{4abK_n + b^2K_t} + \frac{1}{4\mu_b} + \frac{1}{4(\lambda'_b + \mu_b)}, \tag{2-2}$$

$$\frac{1}{E_2} = \frac{1}{aK_n} + \frac{1}{4\mu_b} + \frac{1}{4(\lambda'_b + \mu_b)}, \tag{2-3}$$

$$\frac{1}{G} = \frac{1}{aK_t} + \frac{4a}{b^2K_n + 4abK_t} + \frac{1}{\mu_b}, \tag{2-4}$$

$$\frac{\nu_{12}}{E_1} = \frac{\nu_{21}}{E_2} = \frac{\lambda'_b}{4\mu_b(\lambda'_b + \mu_b)}. \tag{2-5}$$

As pointed out in [Mistler et al. 2007], the out-of-plane constants in (2-1) should be different from the in-plane ones, but the approximation introduced when considering the in-plane constants is reasonable.

**2B. Macroscopic strength condition.** A homogenization procedure for determining the overall yield strength properties of a thin periodic heterogeneous plate was proposed in [Sab 2003; Sab et al. 2007], and applied to masonry walls made of 3D infinitely resistant blocks connected by Mohr–Coulomb interfaces. The procedure provides a smooth representation of the piecewise kinematics of block masonry through

an average strain field. According to these works, the macroscopic strength domain  $G_{\mathbf{t}}$  can be written as

$$G_{\mathbf{t}} := \{\mathbf{t} \mid f^i(\mathbf{t}) \leq 0, \quad \forall i \in [1, \dots, m]\}, \quad (2-6)$$

where  $f^i(\mathbf{t})$  are  $m$  independent planes intersecting in a nonsmooth way:

$$f^i(\mathbf{t}) := \mathbf{n}^i : \mathbf{t} - c^i, \quad i \in [1, \dots, m]. \quad (2-7)$$

and the vector  $\mathbf{n}^i := \partial f^i / \partial \mathbf{t}$  collects the normal to the yield surfaces.

The yield surface comprises  $m = 8$  planes which can be written in terms of stress components in the  $Ox_1x_2$  plane as

$$\begin{aligned} f^1 &:= \mu N_{11} + \operatorname{tg}(\phi) N_{22} + (1 + \operatorname{tg}(\phi)\mu) N_{12} - h \left( c + \frac{c\mu}{\operatorname{tg}(\phi)} \right) \leq 0, \\ f^2 &:= \mu N_{11} + \operatorname{tg}(\phi) N_{22} - (1 + \operatorname{tg}(\phi)\mu) N_{12} - h \left( c - \frac{c\mu}{\operatorname{tg}(\phi)} \right) \leq 0, \\ f^3 &:= N_{22} + \frac{1}{\operatorname{tg}(\phi) N_{12}} - \frac{hc}{\operatorname{tg}(\phi)} \leq 0, \\ f^4 &:= N_{22} - \frac{1}{\operatorname{tg}(\phi) N_{12}} - \frac{hc}{\operatorname{tg}(\phi)} \leq 0, \\ f^5 &:= N_{22} + \frac{2}{h} M_{22} - \frac{hc}{\operatorname{tg}(\phi)} \leq 0, \\ f^6 &:= N_{22} - \frac{2}{h} M_{22} - \frac{hc}{\operatorname{tg}(\phi)} \leq 0, \\ f^7 &:= (p + q) N_{22} + \frac{2}{h} M_{11} - \frac{2}{h} (q - p) M_{22} - \frac{h(p + q)c}{\operatorname{tg}(\phi)} \leq 0, \\ f^8 &:= (p + q) N_{22} - \frac{2}{h} M_{11} - \frac{2}{h} (q - p) M_{22} - \frac{h(p + q)c}{\operatorname{tg}(\phi)} \leq 0, \end{aligned} \quad (2-8)$$

where  $p = (\operatorname{tg}(\phi)/\mu) \cdot (b/4h)$  and  $q = (\operatorname{tg}(\phi)/\mu) \sqrt{1 + (b/4h)^2}$ . The macroscopic strength condition explicitly depends on the aspect ratio  $\mu = 2a/b$  of the blocks, the friction angle  $\phi$  and the cohesion  $c$  of the joints. This latter is included into the formulation and, generally, provided with a very small value, to ensure convergence of the numerical simulations. The strength condition is anisotropic as a consequence of the arrangement of the blocks within the assembly and is unbounded in the direction of compression, according to the hypothesis of infinite crushing strength. As expected, the four planes defining the in-plane strength condition correspond to the macroscopic strength domain obtained in [de Buhan and de Felice 1997].

**2C. Macroscopic elastoplastic constitutive law.** Aiming at building up a constitutive law, let us assume that masonry behaves as an elastic-perfectly plastic homogenized medium with associated flow-rule, having the elastic properties defined in Section 2A and the elastic domain coinciding with the macroscopic strength condition given by (2-6). The model is thus formulated in the framework of infinitesimal multisurface rate-independent elastoplasticity. The total strain  $\boldsymbol{\varepsilon}$  is decomposed additively in an elastic



(reversible) part  $\boldsymbol{\varepsilon}^e$  and a plastic (irreversible) part  $\boldsymbol{\varepsilon}^p$ :

$$\boldsymbol{\varepsilon} = \boldsymbol{\varepsilon}^e + \boldsymbol{\varepsilon}^p. \quad (2-9)$$

By (2-9), the stress-strain relationship can be written as

$$\boldsymbol{t} = \boldsymbol{C} : (\boldsymbol{\varepsilon} - \boldsymbol{\varepsilon}^p), \quad (2-10)$$

where  $\boldsymbol{C} = \boldsymbol{A}^{-1}$  is the elastic stiffness tensor equal to the inverse of the flexibility matrix defined in (2-1).

The previously defined macroscopic strength domain given by equations (2-6)–(2-8) is assumed to coincide with the elastic domain  $E_{\boldsymbol{t}}$ :

$$E_{\boldsymbol{t}} \equiv G_{\boldsymbol{t}} = \{\boldsymbol{t} \mid f^i(\boldsymbol{t}) := \boldsymbol{n}^i : \boldsymbol{t} - c^i \leq 0, \quad \forall i \in [1, \dots, m]\}. \quad (2-11)$$

Accordingly, the boundary of the domain is given by

$$\partial E_{\boldsymbol{t}} := \{\boldsymbol{t} \mid f^i(\boldsymbol{t}) := \boldsymbol{n}^i : \boldsymbol{t} - c^i, \quad \forall i \in [1, \dots, m]\}. \quad (2-12)$$

The evolution of plastic strain  $\boldsymbol{\varepsilon}^p$  is controlled by the associated flow-rule expressed as proposed in [Koiter 1960]:

$$\dot{\boldsymbol{\varepsilon}}^p := \sum_{i=1}^m \dot{\gamma}^i \frac{\partial f^i(\boldsymbol{t})}{\partial \boldsymbol{t}}, \quad (2-13)$$

where  $\dot{\gamma}^i$  are the  $m$  plastic multipliers, subjected to the Kuhn–Tucker conditions for  $i \in [1, \dots, m]$ :

$$\dot{\gamma}^i \geq 0, \quad f^i(\boldsymbol{t}) \leq 0, \quad \dot{\gamma}^i f^i(\boldsymbol{t}) \equiv 0, \quad (2-14)$$

and to the consistency condition  $\dot{\gamma}^i f^i(\boldsymbol{t}) \equiv 0$ .

Equations (2-9)–(2-13) define the constitutive behavior of the material but in order to be used inside the FEM framework, they have to be integrated (see [Simo et al. 1988] for details), obtaining the following equations in terms of finite increments:

$$\boldsymbol{t}_{n+1} = \boldsymbol{C} : (\boldsymbol{\varepsilon}_{n+1} - \boldsymbol{\varepsilon}_{n+1}^p), \quad (2-15)$$

$$\boldsymbol{\varepsilon}_{n+1}^p = \boldsymbol{\varepsilon}_n^p + \sum_{i=1}^m \Delta \gamma_{n+1}^i \frac{\partial f^i(\boldsymbol{t}_{n+1})}{\partial \boldsymbol{t}_{n+1}}, \quad (2-16)$$

where  $n + 1$  denotes the new solutions  $\{\boldsymbol{t}_{n+1}, \boldsymbol{\varepsilon}_{n+1}^p\}$  to be determined with respect to the known state  $\{\boldsymbol{t}_n, \boldsymbol{\varepsilon}_n^p\}$  and the assigned total strain  $\{\boldsymbol{\varepsilon}_{n+1}\}$ . The Kuhn–Tucker conditions in discrete form are expressed as

$$\Delta \gamma_{n+1}^i \geq 0, \quad f^i(\boldsymbol{t}_{n+1}) \leq 0, \quad \Delta \gamma_{n+1}^i f^i(\boldsymbol{t}_{n+1}) = 0, \quad \text{for } i \in [1, \dots, m]. \quad (2-17)$$

As pointed out in [Simo et al. 1988], the solution of the system of equations (2-15)–(2-17), according to the Haar–Karman’s principle, coincides with the following minimization problem:

$$\begin{cases} \text{minimize:} & \Pi_{HK}[\Delta \boldsymbol{t}_{n+1}] = \frac{1}{2}(\Delta \boldsymbol{t}_{n+1} : \boldsymbol{C}^{-1} : \Delta \boldsymbol{t}_{n+1}), \\ \text{subject to:} & f^i(\Delta \boldsymbol{t}_{n+1}) := -\boldsymbol{n}^i : \Delta \boldsymbol{t}_{n+1} - b_{n+1}^i \geq 0, \quad \text{for } i \in [1, \dots, m]. \end{cases} \quad (2-18)$$

Here  $\Delta \mathbf{t} := \mathbf{t} - \mathbf{t}_E$ , where  $\mathbf{t}_E$  the elastic predictor related to the strain increment through the elastic matrix  $\mathbf{C}$ , while  $\mathbf{b}^i := \mathbf{c}^i - \mathbf{n}^i : \mathbf{t}_E$ .

Equation (2-18) represents a standard strictly convex quadratic programming problem expressed in the so-called primal form, where  $\Delta \mathbf{t}_{n+1}$  are the primal variables and the plastic multipliers  $\Delta \gamma_{n+1}$  the dual ones. The approach adopted here for its solution, called dual active set method, was originally proposed in [Goldfarb and Idnani 1983] and then adopted in [Malena and Casciaro 2008] to solve a shakedown structural problem.

### 3. Cracking due to settlement

In this section, the failure pattern in the masonry structure due to ground surface differential settlement is investigated referring to both, a bidimensional façade and a tridimensional building. As suggested in [Portioli and Cascini 2016] and [Mastrodicasa 1993], the foundation settlement is simulated by substituting a part of the foundation by a movable rigid block, connected to the masonry above by a no-tension frictional interface allowing for the possible detachment. By imposing a downward vertical displacement to the movable rigid block, the masonry structure experiences a progressive reduction of the reaction at the basis, up to a limit value corresponding to the self-weight of the portion of the wall involved in the settlement (Figure 4). The resulting failure pattern of masonry is then represented by the plastic strain fields provided by the analyses (Figures 2 and 3). The choice of such a rough simulation of settlement has the advantage of reproducing the same boundary conditions of the well-known experiments carried in [Mastrodicasa 1993] allowing for a direct comparison with them.

**3A. Plane wall.** The first considered masonry wall has a length of 10 m, height of 5 m and a thickness of 0.5 m, while the blocks have a length of 0.5 m, height of 0.25 m and thickness of 0.5 m. The friction coefficient and the unit volume weight are set equal to 0.5 kN/m<sup>3</sup> and 18.0 kN/m<sup>3</sup>, respectively.

Two different settlement configurations were adopted (Figure 2), with a portion of the foundation undergoing a downward displacement having a length of 2 m (short settlement) and 5 m (long settlement).

The vertical reaction at the base of the movable block prior to the application of the settlement is equal to 90.0 kN and 225.0 kN for the two walls, respectively. At failure, the base reactions become equal to 27.8 kN and 152.9 kN (see Figure 4), with a reduction of about 70% and 45%, respectively. The failure patterns are shown in Figure 2 in terms of plastic strain depicted over the deformed configuration of the wall.

The predicted failure patterns are in agreement with the experimental ones presented in [Mastrodicasa 1993]: in both cases the inelastic strain is localised over a diagonal band originating at the boundary between the movable block and the fixed foundation, with an inclination that depends on the aspect ratio of the blocks. In the case of the short settlement (Figure 2, left), the inelastic deformed band terminates on the lateral edge of the wall, while, in case of the long settlement (Figure 2, right), terminates on the top of the wall, with a larger portion of the wall mobilized by the settlement and a corresponding lower decrease in the vertical reaction.

**3B. Wall with openings.** The second masonry wall taken into account has the same geometry as the previous one, but is provided with three orders of openings spanning  $1 \times 1 \text{ m}^2$  (Figure 3). The end settlement 1.5 m long, and the central settlement 5 m long were analyzed. As expected, the presence of



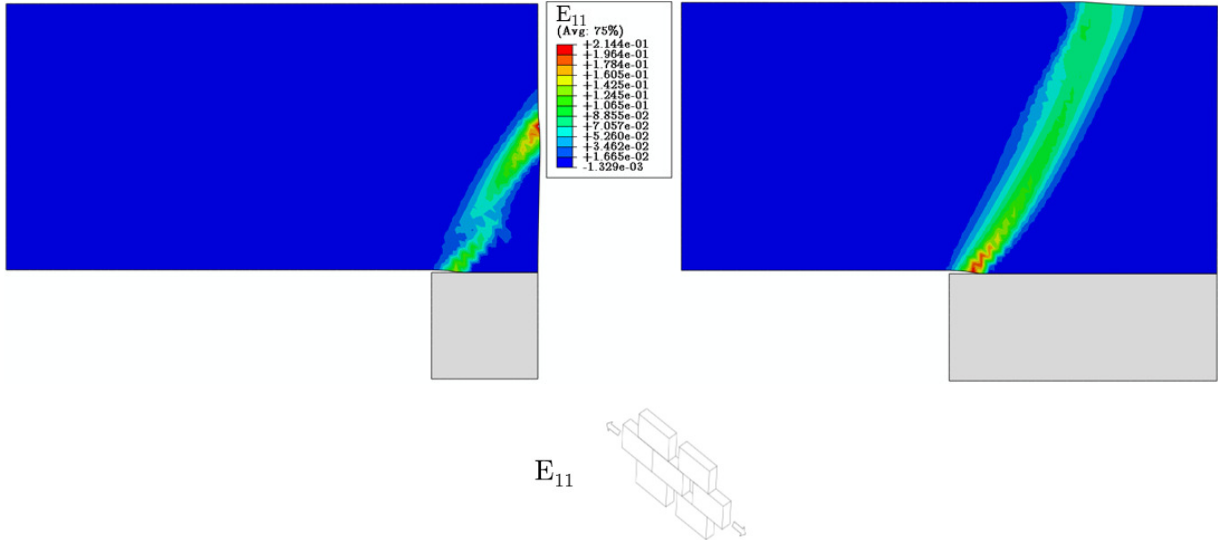


**Figure 2.** Plastic strain distributions at failure: short (left) and long settlement for plane wall (right).

openings introduces discontinuities that affect the strain pattern at failure. The inelastic strains always originate at the boundaries of the portion of the foundation that displaces downwards, but end to localize in the masonry strips over the openings (Figure 3). Clearly, the inelastic strain pattern depend on how the lintels are modelled. In both cases the displacement of the wall can be described as a rigid body vertical translation of the pier lying over the movable foundation. The relative displacement of the pier with the rest of the structure is then accommodated through the inelastic strain concentrating over the horizontal masonry strips between the openings adjacent to the pier.

The base reaction versus the vertical support displacement is plotted in Figure 4 (right): almost no reduction is obtained in the case of the end settlement, since the subsidence of the pier does not involve a significant redistribution of the load towards the adjacent masonry.

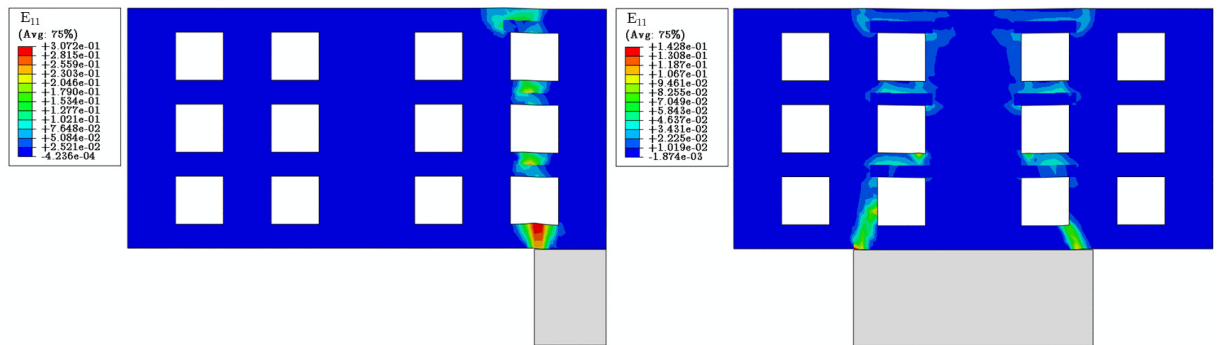


**Figure 3.** Plastic strain distributions at failure: end settlement for wall with openings (left) and central settlement for wall with openings (right).

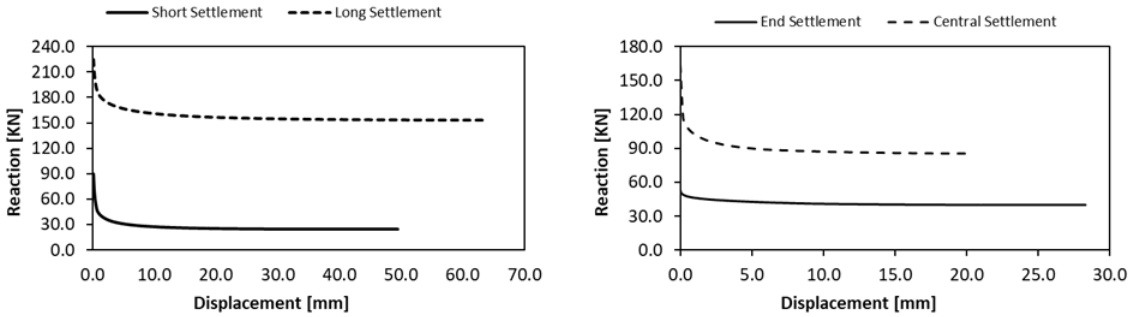


**Figure 4.** Base reaction versus vertical support displacement for full wall (left) and wall with openings (right).

**3C. 3D building.** Aiming at testing the capability of the proposed model to catch the three dimensional behavior, a small two-story masonry building is considered made of four connected walls. The considered 3D building (Figure 5) is the same as the one proposed in [Portioli and Cascini 2016]. The front façade includes two doors at the ground floor and two windows at the first floor having timber lintels above the openings. The size of a single brick is 80 mm × 40 mm × 30 mm (length, height, thickness). The friction coefficient is set equal to 0.5, while the unit weights of masonry and timber are equal to 26.8 kN/m<sup>3</sup> and 6.0 kN/m<sup>3</sup>, respectively.

The settlement was imposed through the application of a vertical downward displacement at the right corner of the building, including the central wall of the façade between the openings and half of the lateral wall (see Figure 5, left). The inelastic strain field, as depicted in Figure 5 (right), results in a good agreement with the corresponding analysis on the discrete masonry assembly shown in [Portioli and Cascini 2016], demonstrating the capability of the proposed model to provide a reliable prediction of the expected failure mode. The vertical reaction at the base of the movable support decreases from 1.027 kN, before the settlement, up to 0.659 kN when the plastic flow occurs.

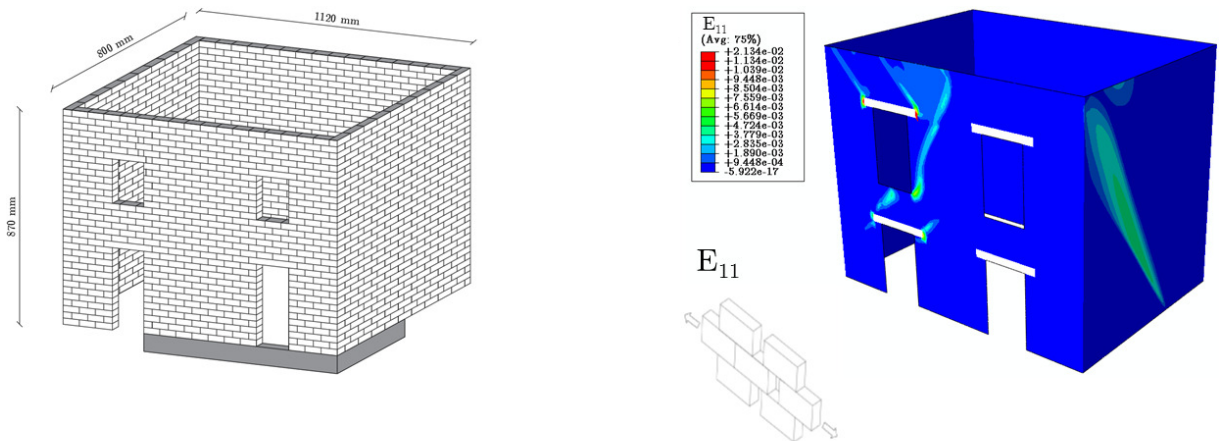


**Figure 5.** 3D building subject to foundation settlement: geometrical characteristics (left) and plastic strain distribution at failure (right).

#### 4. Cracking due to earthquake

This section aims at assessing the capability of the model in providing a prediction of the expected failure modes of masonry buildings under earthquake loading. To this end, as frequently proposed in the literature, the earthquake load is simply represented by horizontal body forces increasing up to the attainment of the failure mechanism. Some preliminary benchmark are carried out, aiming at describing how the model behaves under out-of-plane loads, and then some more complex geometries are investigated and the results compared to the tilting tests carried out in [Restrepo Vélez et al. 2014] on 1 : 5 scale on dry-stone masonry.

**4A. Preliminary benchmarks.** The first benchmark, originally proposed in [Cecchi et al. 2007], consists of a rectangular panel subjected to self-weight and to increasing horizontal out-of-plane distributed load. The wall has a length of 3 m, height 3 m and a thickness of 30 cm. It is simply supported at the base and restrained at the top against out-of-plane displacement. The blocks are 20 cm  $\times$  10 cm  $\times$  30 cm. The unit weight of masonry is equal to 20 kN/m<sup>3</sup>, while the friction coefficient and the cohesion in the joints are equal to 0.471 N/mm<sup>2</sup> and 0.1 N/mm<sup>2</sup>, respectively.

The results of the analysis are provided in Figure 6 in terms of plastic strain component  $\chi_{22}$ , corresponding to the curvature along the vertical direction, and in terms of vertical displacement  $u_2$ . The horizontal load at failure is equal to 1.421 N/cm<sup>2</sup>, while the plastic hinge develops at 184 cm from the ground. The solution shows the uplift of the wall, as a consequence of the fact that the horizontal plastic hinge does not arise in the middle-plane but on the external surface, as it actually occurs in masonry walls. The results are well in accordance with those provided in [Cecchi et al. 2007].

As a second benchmark, two masonry panels experimentally tested in [Southcombe et al. 1995; Chong et al. 1994] have been numerically simulated. The panels, having dimensions 5625 mm  $\times$  2465 mm  $\times$  102.5 mm, were loaded by air-bags up to failure with increasing uniform lateral pressure. They are fully clamped at the base and free on the top, while both lateral edges are simply supported, as shown in Figure 7 (second row).

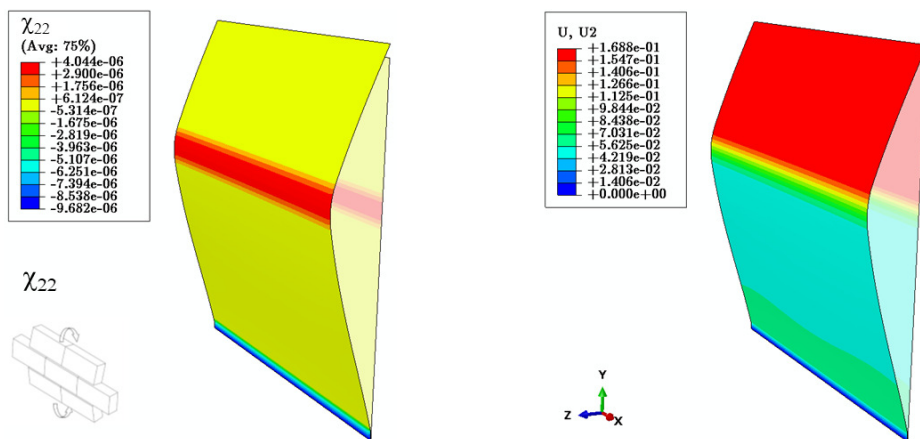


**Figure 6.** Plastic strain distribution (left) and vertical displacement (right) at failure.

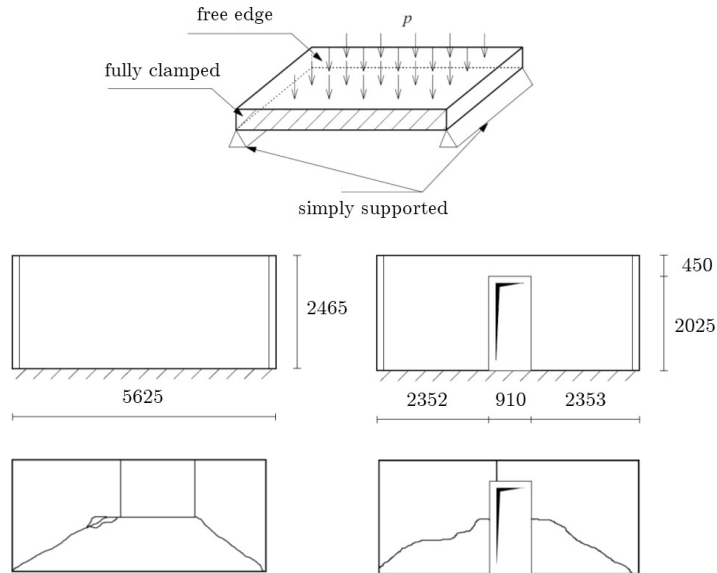


**Figure 7.** Masonry panels experimentally tested in [Southcombe et al. 1995; Chong et al. 1994]: geometry (second row) and failure patterns (third row).

Each panel consists of solid clay bricks having dimensions  $215 \text{ mm} \times 65 \text{ mm} \times 102.5 \text{ mm}$ , and mortar joints with thickness  $10 \text{ mm}$ . The pressure at failure provided by the experiments is equal to  $2.8 \text{ kN/m}^2$  and  $2.2 \text{ kN/m}^2$  for the plane wall (SB01 test) and for the wall with the opening (SB04 test), respectively. The numerical simulations have been carried out assuming a cohesion equal to  $0.32 \text{ MPa}$  and a friction angle equal to  $36^\circ$ . The pressure at failure provided by the model is equal to  $2.71 \text{ kN/m}^2$  and  $2.49 \text{ kN/m}^2$  for the SB01 and SB04 tests, respectively. The plastic strain component  $\chi_{11}$ , corresponding to the curvature along the horizontal direction, is represented in Figure 8, showing a reasonable matching with the experimental crack pattern (Figure 7, third row).

**4B. Tilting tests.** In this section, the capability of the model in reproducing the failure mechanisms obtained in the experimental campaign carried out in [Restrepo Vélez et al. 2014] are described. The experimental campaign consists in  $1 : 5$  scale dry-stone masonry walls built over a tilting table and tested up to failure. Each prototype was first built under the self-weight and then brought up to failure by tilting the table. The horizontal collapse multiplier is simply the tangent of the table tilt angle causing the collapse. The walls are made of dry-stone bricks, with specific weight  $26.8 \text{ kN/m}^3$  and dimensions of  $30 \text{ mm} \times 80 \text{ mm} \times 40 \text{ mm}$ . The friction coefficient ranges from  $0.67$  to  $0.77$ , as shown in [Restrepo Vélez et al. 2014]. Several configurations were tested, consisting in three U-shaped walls made of an out-of-plane loaded wall constrained at both lateral edges by in-plane loaded walls, having different length and vertical loading at the top. The numerical simulations are carried out by reproducing the same geometry, assuming a friction coefficient of  $0.7$  and neglecting the cohesion, while the load condition is enforced by constraining the walls at their base, activating the self-weight and then applying increasing horizontal body forces, up to failure, while recording the horizontal collapse multiplier  $\lambda_c$  equal to the ratio between horizontal and vertical body forces.

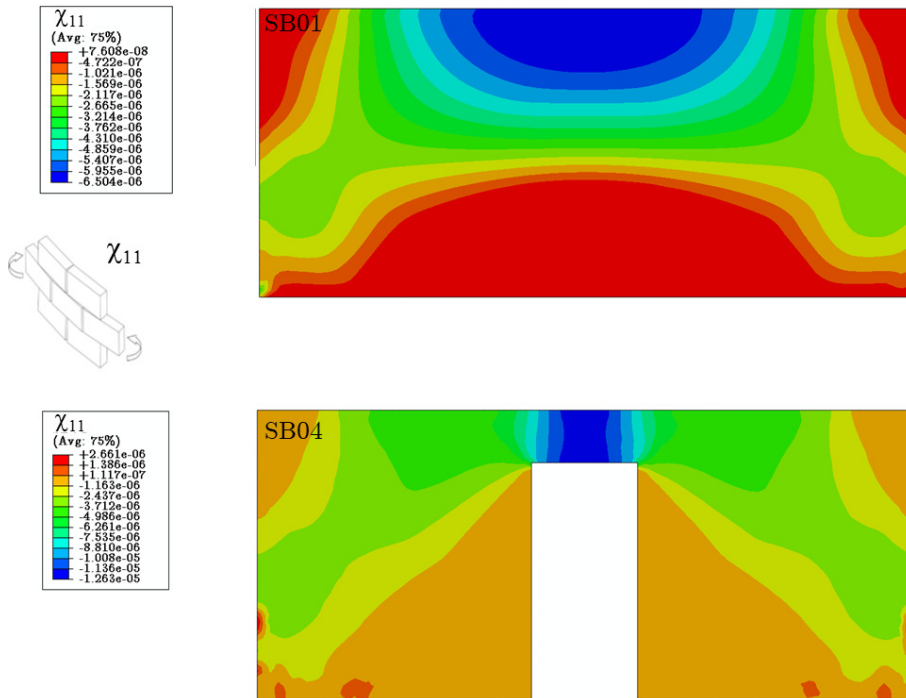


**Figure 8.** Plastic strain distributions at failure for tests SB01 (top) and SB04 (bottom).

**4B.1. U-shaped walls loaded inward.** The first experimental test named S1 [Restrepo Vélez et al. 2014] consists of a wall with a length of 11 bricks and a height of 21 bricks, loaded inward and restrained by two lateral side walls having the same height and a length of 4 bricks (Figure 9, top). The test was repeated three times, providing an average value of the collapse multiplier equal to 0.241, while the numerical prediction is equal to 0.284 with an overestimate of about 18%. The predicted versus experimental failure modes are compared in Figure 9, resulting in a good reproduction of the failure pattern, with the inelastic strain component  $\chi_{11}$  corresponding to the opening of the head joints in the upper central portion of the main wall and at the corner with the side walls.

**4B.2. U-shaped walls loaded outward.** The three experimental tests S7, S10 and S20 are similar to the previous S1 test but with the front wall loaded outwards. The three specimens have the same height of 21 bricks but differ in the length of the walls: the specimen S7 has the out-of-plane loaded front wall made of 8 bricks and the side walls of 7 bricks; the specimen S10 has the front wall made of 12 bricks and the side walls of 10 bricks; the specimen S20 has the front wall made of 14 bricks and the side walls of 10 bricks, with a further central transversal wall similar to the side walls (see the figures 10 (top), 11 (top) and 12 (top)). The experimental collapse horizontal multipliers are equal to 0.291, 0.231 and 0.285, while those predicted by the model are equal to 0.287, 0.241 and 0.262 for test S7, S10 and S20, respectively, with a discrepancy of about  $-1\%$ ,  $+7\%$  and  $-8\%$ .

The failure modes depend on the length-to-height ratio of the front wall: for shorter wall length the failure is driven by the in-plane diagonal cracking of the side walls, while for greater wall length the failure is controlled by out-of-plane bending of the front wall. Both inelastic phenomena are correctly

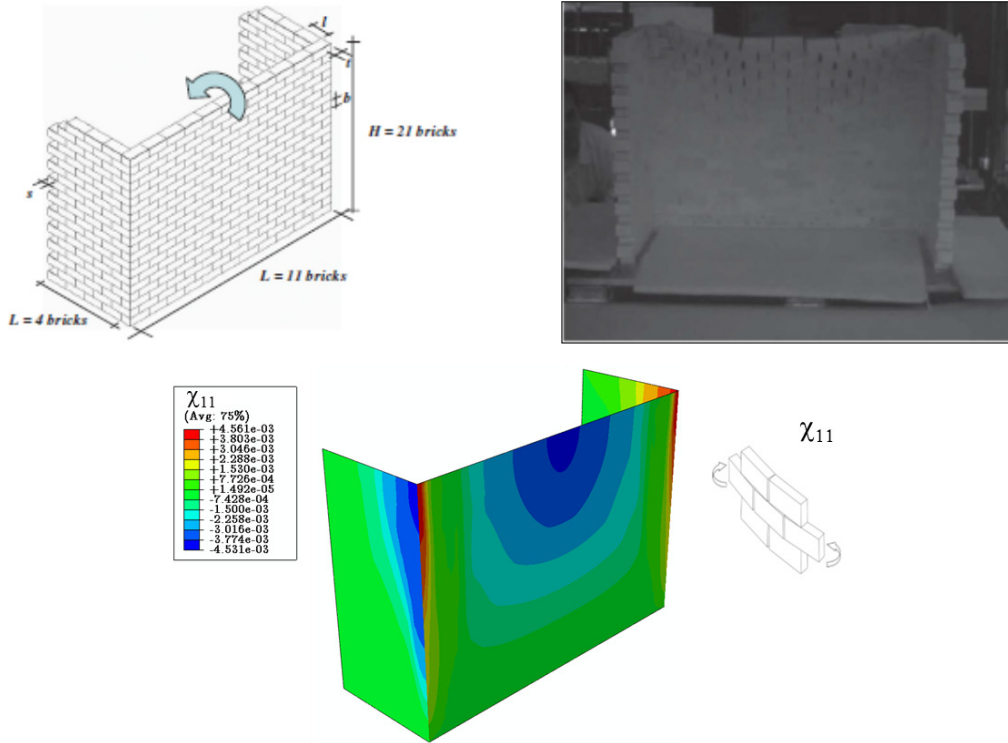


**Figure 9.** Test S1: experimental ( $\lambda_{exp} = 0.241$ ) [Restrepo Vélez et al. 2014] (top) versus numerical results ( $\lambda = 0.284$ ) (bottom).

simulated by the numerical analyses as shown by the plastic strain field represented in figures 10, 11 and 12, resulting in a good agreement with experimental results. More precisely, in test S7, failure is reached through overturning of the upper part of the front wall, with a horizontal hinge forming at about half of its height, while the side walls display opening of the head joints and sliding of the bricks. Both phenomena are nicely simulated by the inelastic strain components  $\chi_{22}$  related to curvature in the vertical direction and  $E_{11}$ , related to the opening of the head joints, as shown in Figure 10. In test S10, the out-of-plane displacement of the front wall is accompanied by a more pronounced bending deformation, with the  $\chi_{11}$  inelastic curvature localised at the upper central portion of the front wall (Figure 11). In test S20, the failure pattern displays a mixed failure mode including both, overturning and out-of-plane bending, associated with in-plane diagonal cracking in the transversal walls, especially in the central one (Figure 12).

**4B.3. Effect of vertical load.** The Specimens S32 and S41 were tested to study the effect of overburden forces and restrains coming from floor joists (figures 13, top and 14, top). The specimen S32 consists in a simple wall with a length of 14 bricks and height of 21 bricks restrained at the top by means of the floor joists which also apply a vertical load on the wall of about 181 N.

The specimen S41 consists in three U-shaped walls with a height of 21 bricks, comprising two side walls with a length of 8 brick and a front wall with a length of 10 bricks restrained at the top, as in the previous case, and subjected to a vertical load of about 115 N (Figure 14, top).



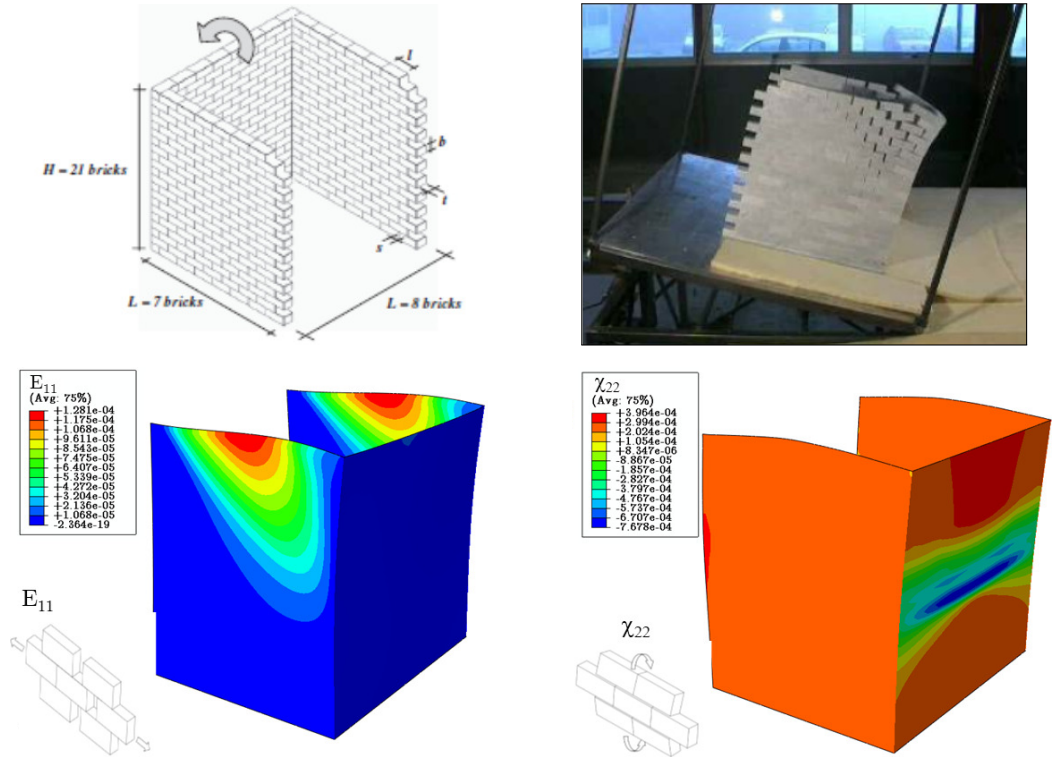


**Figure 10.** Test S7: experimental ( $\lambda_{\text{exp}} = 0.291$ ) [Restrepo Vélez et al. 2014] (top) versus numerical results ( $\lambda = 0.287$ ) (bottom).

The collapse multipliers resulting from the experiments are equal to 0.293 and 0.423, while the numerical predictions are equal to 0.285 and 0.413, for tests S32 and S41, respectively, with a slight underestimate of about 3% for both the simulations.

For the test S32, the failure pattern consists in the vertical bending around two horizontal hinges forming at the base and at about 3/4 of the height of the wall. The numerical results (see Figure 13) provide a strong concentration of the inelastic curvature  $\chi_{22}$  that matches perfectly to the flexural opening in the bed joints at the intermediate hinge.

Numerical and experimental results for test S41 are compared in Figure 14. The failure pattern on the front wall is similar to the previous case, but the hinge is much higher, at about 80% of the height of the wall. On the lateral side walls the bricks slide and the vertical joints open along a diagonal crack that is well represented by the inelastic strain component  $E_{11}$  resulting from the numerical simulations.

**4B.4. 3D Building.** As a final benchmark, the test S42 was simulated by numerical analysis, aiming at reproducing the behavior of a two-story 3D building. The geometry of the specimen consists in a masonry cell made of four connected walls with a height of 42 bricks and a length of 10 and 13 bricks. Two opposite walls are provided with four openings each. The collapse multiplier measured in the laboratory was equal to 0.236, while the numerical prediction is equal to 0.226, with a slight underestimate of about 4%.

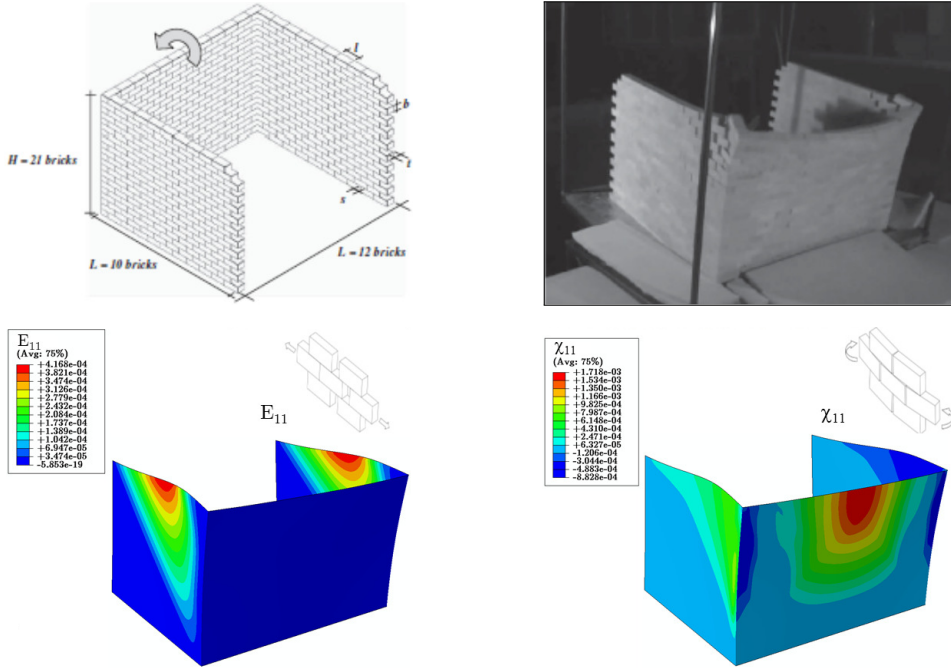


Figure 11. Test S10: experimental ( $\lambda_{exp} = 0.231$ ) [Restrepo Vélez et al. 2014] (top) versus numerical results ( $\lambda = 0.241$ ) (bottom).

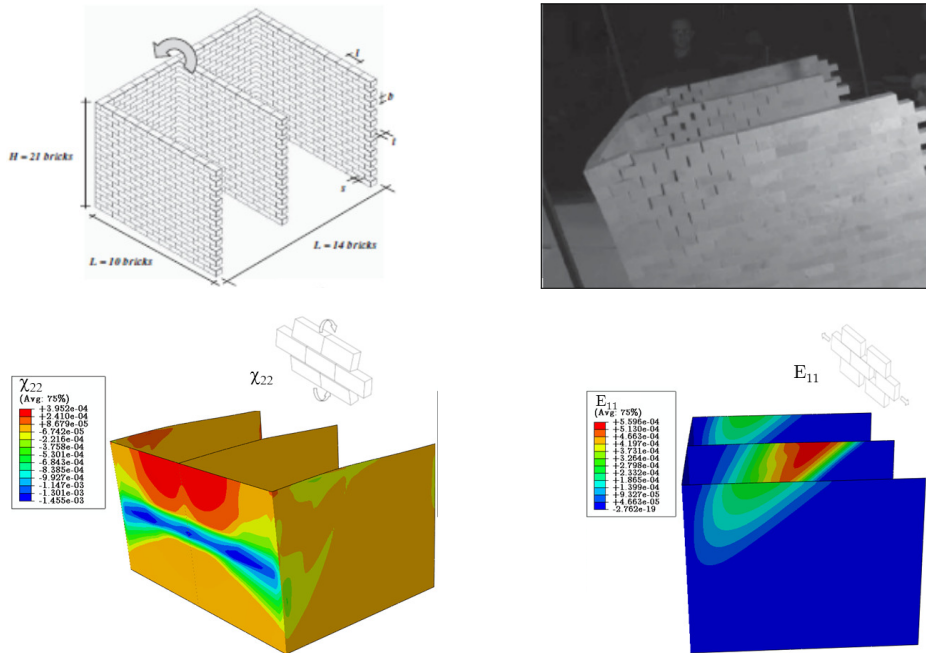
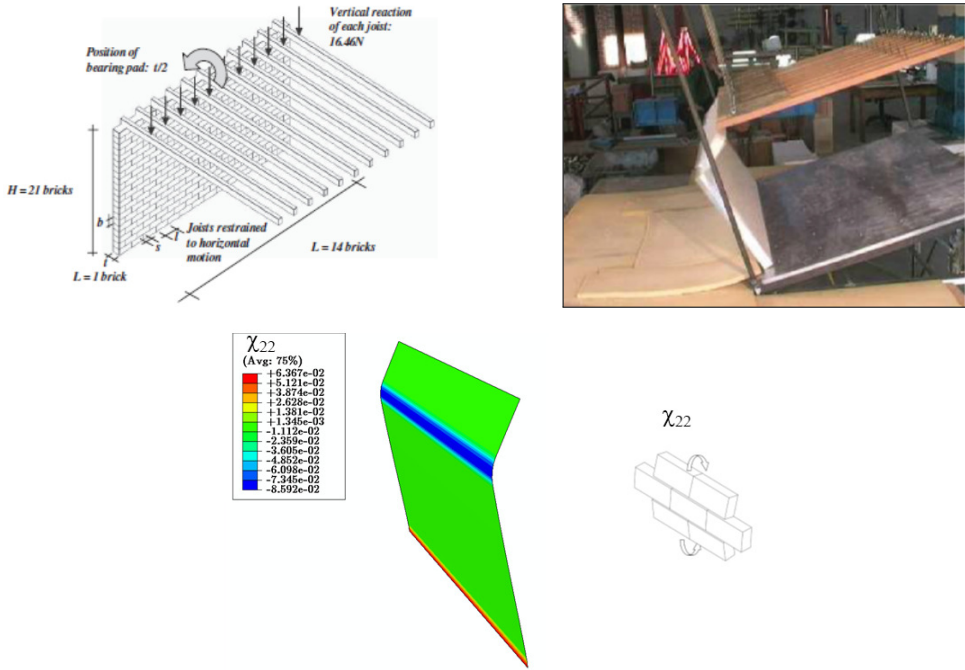
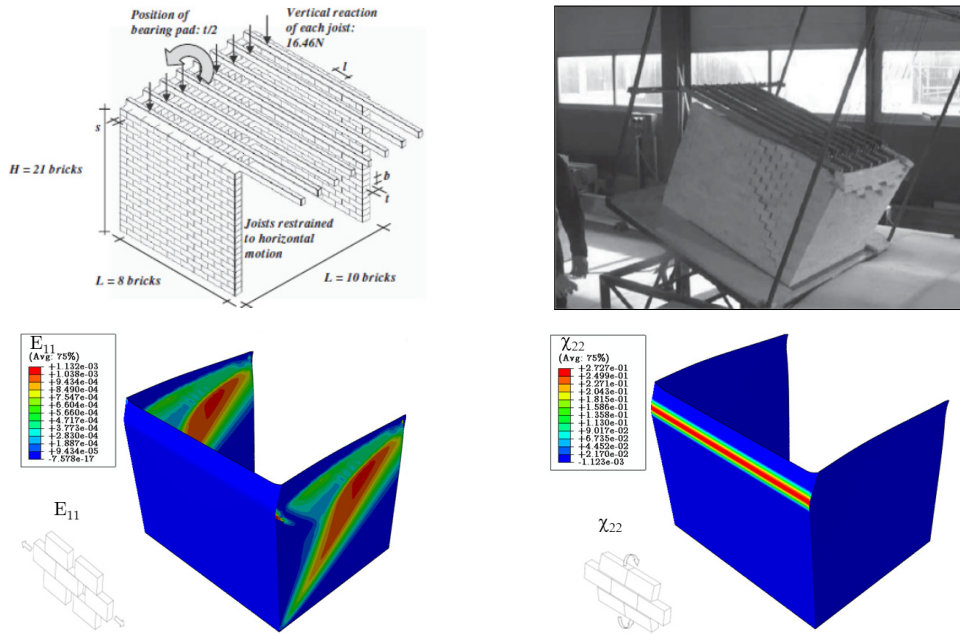


Figure 12. Test S20: experimental ( $\lambda_{exp} = 0.285$ ) [Restrepo Vélez et al. 2014] (top) versus numerical results ( $\lambda = 0.262$ ) (bottom).



**Figure 13.** Test S32: experimental ( $\lambda_{exp} = 0.293$ ) [Restrepo Vélez et al. 2014] (top) versus numerical results ( $\lambda = 0.285$ ) (bottom).



**Figure 14.** Test S41: experimental ( $\lambda_{exp} = 0.423$ ) [Restrepo Vélez et al. 2014] (top) versus numerical results ( $\lambda = 0.413$ ) (bottom).

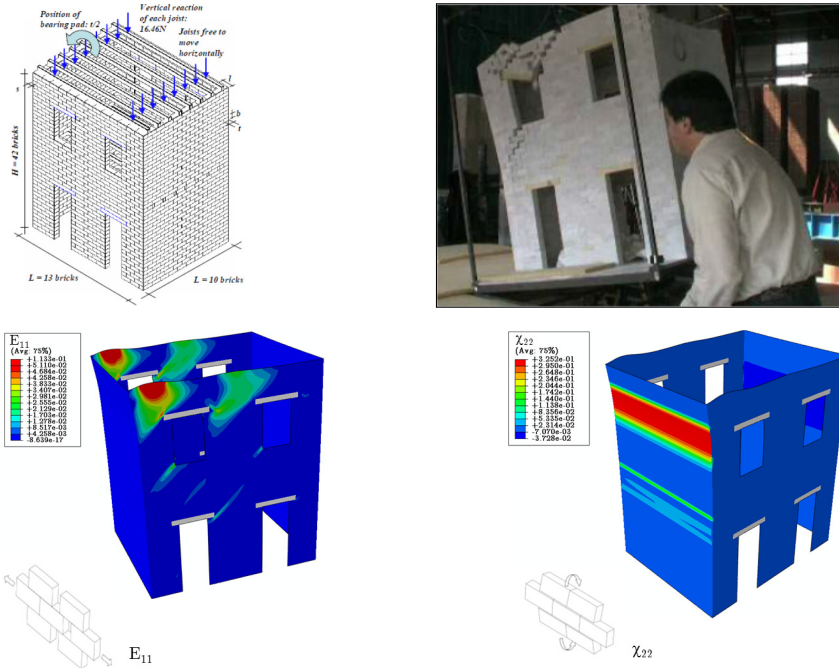


**Figure 15.** Test S42: experimental ( $\lambda_{exp} = 0.236$ ) [Restrepo Vélez et al. 2014] (top) versus numerical results ( $\lambda = 0.226$ ) (bottom).

The failure pattern concentrates at the left upper top of the specimen, close to the opening, with the appearance of a diagonal crack originating at the lower left corner and at the upper right corner of the lateral opening (Figure 15). Once again, the crack pattern provided by the experiments is well reproduced by the inelastic strain field predicted by the numerical analyses. Referring to Figure 15 (bottom), the horizontal strain component  $E_{11}$  tends to localise in accordance with the opening of the head joints in the in-plane loaded walls, while the vertical curvature  $\chi_{22}$ , reproduces the horizontal hinges corresponding to the overturning of the upper part of the out-of-plane loaded walls.

As a summary of the tests under horizontal loading, it is worth noting that the numerical outcomes of the tests controlled by the in-plane behavior (i.e., S7, S22, S32, S41 and S42) match quite well the experimental results in terms of failure load. Conversely, the numerical outcomes for tests S1 and S10 are affected by a larger discrepancy. The difference can be ascribed to the simplicity of the model adopted for the definition of the strength domain [Sab 2003], which overestimate the load multiplier when torsional behavior is involved.

### 5. Conclusion

A continuous finite element model for the nonlinear analysis of ancient masonry buildings is developed, implemented in a finite element code and applied to the assessment of masonry buildings subjected either to foundation settlements or to lateral seismic loads. The model is validated by comparison with the experimental results in terms of failure pattern and ultimate live load. The comparison shows the ability of the model in predicting the failure pattern with different loading and boundary conditions.

Accordingly, the expected collapse mechanism is a result of the analysis and does not have to be a-priori defined, as suggested by current assessment procedures. The model is based on few parameters, namely a mechanical parameter consisting in the friction coefficient of the joints and a geometrical parameter consisting in the aspect ratio of the blocks, that can be easily evaluated in existing masonry structures. It should be noticed that more refined models are available in the literature that are based on advanced constitutive laws including softening, cracking and describing more accurately the nonlinear mechanical behavior of masonry. However, the use of such models generally requires many data input, which are often hardly available in current practice and a strong computational effort for application to real structures. In this perspective, the nonlinear model presented in this study might represent a good compromise in terms of accuracy of the results, available input data, and computational cost. For this reason, the proposed numerical approach represents a promising tool for the analysis of historic masonry buildings under foundation settlements or earthquake loads.

### Acknowledgements

The present work was supported by the research grant SiCura 2018-2020 funded by the Regione Lazio and by the research grant DPC-ReLUIIS 2019-2021 funded by the Italian Civil Protection Department.

### References

- [Acito et al. 2016] M. Acito, C. Chesi, G. Milani, and S. Torri, “Collapse analysis of the clock and fortified towers of Finale Emilia, Italy, after the 2012 Emilia Romagna seismic sequence: lesson learned and reconstruction hypotheses”, *Constr. Build. Mater.* **115** (2016), 193–213.
- [Amorosi et al. 2012] A. Amorosi, D. Boldini, G. de Felice, and M. Malena, “Tunnelling-induced deformation on a masonry structure: a numerical approach”, pp. 353–359 in *Geotechnical aspects of underground construction in soft ground* (Rome, 2011), edited by G. Viggiani, Taylor & Francis, London, 2012.
- [Amorosi et al. 2014] A. Amorosi, D. Boldini, G. de Felice, M. Malena, and M. Sebastianelli, “Tunnelling-induced deformation and damage on historical masonry structures”, *Géotechnique* **64**:2 (2014), 118–130.
- [Angelillo 1993] M. Angelillo, “Constitutive relations for no-tension materials”, *Meccanica (Milano)* **28**:3 (1993), 195–202.
- [Angelillo et al. 2010] M. Angelillo, L. Cardamone, and A. Fortunato, “A numerical model for masonry-like structures”, *J. Mech. Mater. Struct.* **5**:4 (2010), 583–615.
- [de Buhan and de Felice 1997] P. de Buhan and G. de Felice, “A homogenization approach to the ultimate strength of brick masonry”, *J. Mech. Phys. Solids* **45**:7 (1997), 1085–1104.
- [Caillerie 1984] D. Caillerie, “Thin elastic and periodic plates”, *Math. Methods Appl. Sci.* **6**:2 (1984), 159–191.
- [Calió et al. 2012] I. Calió, M. Marletta, and B. Pantó, “A new discrete element model for the evaluation of the seismic behaviour of unreinforced masonry buildings”, *Eng. Struct.* **40** (2012), 327–338.
- [Cecchi and Sab 2002] A. Cecchi and K. Sab, “A multi-parameter homogenization study for modeling elastic masonry”, *Eur. J. Mech. A Solids* **21**:2 (2002), 249–268.
- [Cecchi et al. 2007] A. Cecchi, G. Milani, and A. Tralli, “A Reissner–Mindlin limit analysis model for out-of-plane loaded running bond masonry walls”, *Int. J. Solids Struct.* **44**:5 (2007), 1438–1460.
- [Chong et al. 1994] V. L. Chong, C. Southcombe, and I. M. May, “The behaviour of laterally loaded masonry panels with openings”, pp. 178–182 in *Masonry* (London, 1992), edited by H. W. H. West, Proc. British Masonry Soc. **6**, Brit. Masonry Soc., Stoke-on-Trent, UK, 1994.
- [de Felice 1995] G. de Felice, “Détermination des coefficients d'élasticité de la maçonnerie par une méthode d'homogénéisation”, pp. 393–396 in *Actes du 12ème Congrès Français de Mécanique, I* (Strasbourg, 1995), Assoc. Univ. Mécanique, Strasbourg, 1995.



- [de Felice 2001] G. de Felice, “Overall elastic properties of brickwork via homogenization”, pp. 411–418 in *Structural engineering, mechanics, and computation, I* (Cape Town, 2001), edited by A. Zingoni, Elsevier, 2001.
- [de Felice et al. 2010] G. de Felice, A. Amorosi, and M. Malena, “Elasto-plastic analysis of block structures through a homogenization method”, *Int. J. Numer. Anal. Methods Geomech.* **34**:3 (2010), 221–247.
- [de Felice et al. 2017] G. de Felice, S. de Santis, P. B. Lourenço, and N. Mendes, “Methods and challenges for the seismic assessment of historic masonry structures”, *Int. J. Archit. Herit.* **11**:1 (2017), 143–160.
- [Goldfarb and Idnani 1983] D. Goldfarb and A. Idnani, “A numerically stable dual method for solving strictly convex quadratic programs”, *Math. Program.* **27**:1 (1983), 1–33.
- [Heyman 1966] J. Heyman, “The stone skeleton”, *Int. J. Solids Struct.* **2**:2 (1966), 249–279.
- [Koiter 1960] W. T. Koiter, “General theorems for elastic-plastic solids”, pp. 165–221 in *Progress in solid mechanics*, edited by I. N. Sneddon and R. Hill, North-Holland, Amsterdam, 1960.
- [Livesley 1978] R. K. Livesley, “Limit analysis of structures formed from rigid blocks”, *Int. J. Numer. Methods Eng.* **12**:12 (1978), 1853–1871.
- [Lourenço and Ramos 2004] P. B. Lourenço and L. F. Ramos, “Characterization of cyclic behavior of dry masonry joints”, *J. Struct. Eng. (ASCE)* **130**:5 (2004), 779–786.
- [Malena and Casciaro 2008] M. Malena and R. Casciaro, “Finite element shakedown analysis of reinforced concrete 3D frames”, *Comput. Struct.* **86**:11-12 (2008), 1176–1188.
- [Malena et al. 2019] M. Malena, F. Portioli, R. Gagliardo, G. Tomaselli, L. Cascini, and G. de Felice, “Collapse mechanism analysis of historic masonry structures subjected to lateral loads: a comparison between continuous and discrete models”, *Comput. Struct.* **220** (2019), 14–31.
- [Massart et al. 2005] T. J. Massart, R. H. J. Peerlings, M. G. D. Geers, and S. Gottcheiner, “Mesoscopic modeling of failure in brick masonry accounting for three-dimensional effects”, *Eng. Fract. Mech.* **72**:8 (2005), 1238–1253.
- [Mastrodicasa 1993] S. Mastrodicasa, *Dissesti statici delle strutture edilizie*, 9th ed., Hoepli, Milan, 1993.
- [Milani et al. 2006a] G. Milani, P. B. Lourenço, and A. Tralli, “Homogenised limit analysis of masonry walls, I: Failure surfaces”, *Comput. Struct.* **84**:3-4 (2006), 166–180.
- [Milani et al. 2006b] G. Milani, P. B. Lourenço, and A. Tralli, “Homogenised limit analysis of masonry walls, II: Structural examples”, *Comput. Struct.* **84**:3-4 (2006), 181–195.
- [Milani et al. 2007] G. Milani, P. B. Lourenço, and A. Tralli, “3D homogenized limit analysis of masonry buildings under horizontal loads”, *Eng. Struct.* **29**:11 (2007), 3134–3148.
- [Mistler et al. 2007] M. Mistler, A. Anthoine, and C. Butenweg, “In-plane and out-of-plane homogenisation of masonry”, *Comput. Struct.* **85**:17-18 (2007), 1321–1330.
- [Page 1978] A. W. Page, “Finite element model for masonry”, *J. Struct. Div. (ASCE)* **104**:8 (1978), 1267–1285.
- [Pande et al. 1989] G. N. Pande, J. X. Liang, and J. Middleton, “Equivalent elastic moduli for brick masonry”, *Comput. Geotech.* **8**:3 (1989), 243–265.
- [Pietruszczak and Niu 1992] S. Pietruszczak and X. Niu, “A mathematical description of macroscopic behaviour of brick masonry”, *Int. J. Solids Struct.* **29**:5 (1992), 531–546.
- [Portioli and Cascini 2016] F. Portioli and L. Cascini, “Assessment of masonry structures subjected to foundation settlements using rigid block limit analysis”, *Eng. Struct.* **113** (2016), 347–361.
- [Portioli et al. 2014] F. Portioli, C. Casapulla, M. Gilbert, and L. Cascini, “Limit analysis of 3D masonry block structures with non-associative frictional joints using cone programming”, *Comput. Struct.* **143** (2014), 108–121.
- [Restrepo Vélez et al. 2014] L. F. Restrepo Vélez, G. Magenes, and M. C. Griffith, “Dry stone masonry walls in bending, I: Static tests”, *Int. J. Archit. Herit.* **8**:1 (2014), 1–28.
- [Roselli et al. 2018] I. Roselli, M. Malena, M. Mongelli, N. Cavalagli, M. Gioffrè, G. De Canio, and G. de Felice, “Health assessment and ambient vibration testing of the ‘Ponte delle Torri’ of Spoleto during the 2016-2017 Central Italy seismic sequence”, *J. Civ. Struct. Health Monit.* **8**:2 (2018), 199–216.
- [Sab 2003] K. Sab, “Yield design of thin periodic plates by a homogenization technique and an application to masonry walls”, *C. R. Mécanique* **331**:9 (2003), 641–646.



- [Sab et al. 2007] K. Sab, J. Dallot, and A. Cecchi, “Determination of the overall yield strength domain of out-of-plane loaded brick masonry”, *Int. J. Multiscale Comput. Eng.* **5**:2 (2007), 83–92.
- [Sacco 2009] E. Sacco, “A nonlinear homogenization procedure for periodic masonry”, *Eur. J. Mech. A Solids* **28**:2 (2009), 209–222.
- [Simo et al. 1988] J. C. Simo, J. G. Kennedy, and S. Govindjee, “Nonsmooth multisurface plasticity and viscoplasticity: loading/unloading conditions and numerical algorithms”, *Int. J. Numer. Methods Eng.* **26**:10 (1988), 2161–2185.
- [Southcombe et al. 1995] C. Southcombe, I. M. May, and V. L. Chong, “The behaviour of brickwork panels with openings under lateral load”, pp. 105–110 in *Masonry*, edited by H. W. H. West, Proc. British Masonry Soc. **7**, Brit. Masonry Soc., Stoke-on-Trent, UK, 1995.
- [Stefanou et al. 2015] I. Stefanou, K. Sab, and J.-V. Heck, “Three dimensional homogenization of masonry structures with building blocks of finite strength: a closed form strength domain”, *Int. J. Solids Struct.* **54** (2015), 258–270.
- [Taliercio 2016] A. Taliercio, “Closed-form expressions for the macroscopic flexural rigidity coefficients of periodic brickwork”, *Mech. Res. Commun.* **72** (2016), 24–32.
- [Zucchini and Lourenço 2002] A. Zucchini and P. B. Lourenço, “A micro-mechanical model for the homogenisation of masonry”, *Int. J. Solids Struct.* **39**:12 (2002), 3233–3255.

Received 26 Nov 2018. Revised 16 Sep 2019. Accepted 28 Sep 2019.

GIANMARCO DE FELICE: [defelice@uniroma3.it](mailto:defelice@uniroma3.it)

Department of Engineering, Roma Tre University, via Vito Volterra 62, 00146 Rome, Italy

MARIALAURA MALENA: [marialaura.malena@uniroma3.it](mailto:marialaura.malena@uniroma3.it)

Department of Engineering, Roma Tre University, via Vito Volterra 62, 00146 Rome, Italy

# JOURNAL OF MECHANICS OF MATERIALS AND STRUCTURES

[msp.org/jomms](http://msp.org/jomms)

Founded by Charles R. Steele and Marie-Louise Steele

## EDITORIAL BOARD

ADAIR R. AGUIAR	University of São Paulo at São Carlos, Brazil
KATIA BERTOLDI	Harvard University, USA
DAVIDE BIGONI	University of Trento, Italy
MAENGHYO CHO	Seoul National University, Korea
HUILING DUAN	Beijing University
YIBIN FU	Keele University, UK
IWONA JASIUK	University of Illinois at Urbana-Champaign, USA
DENNIS KOCHMANN	ETH Zurich
MITSUTOSHI KURODA	Yamagata University, Japan
CHEE W. LIM	City University of Hong Kong
ZISHUN LIU	Xi'an Jiaotong University, China
THOMAS J. PENCE	Michigan State University, USA
GIANNI ROYER-CARFAGNI	Università degli studi di Parma, Italy
DAVID STEIGMANN	University of California at Berkeley, USA
PAUL STEINMANN	Friedrich-Alexander-Universität Erlangen-Nürnberg, Germany
KENJIRO TERADA	Tohoku University, Japan

## ADVISORY BOARD

J. P. CARTER	University of Sydney, Australia
D. H. HODGES	Georgia Institute of Technology, USA
J. HUTCHINSON	Harvard University, USA
D. PAMPLONA	Universidade Católica do Rio de Janeiro, Brazil
M. B. RUBIN	Technion, Haifa, Israel

**PRODUCTION** [production@msp.org](mailto:production@msp.org)

SILVIO LEVY Scientific Editor


Cover photo: Mando Gomez, [www.mandolux.com](http://www.mandolux.com)

See [msp.org/jomms](http://msp.org/jomms) for submission guidelines.

JoMMS (ISSN 1559-3959) at Mathematical Sciences Publishers, 798 Evans Hall #6840, c/o University of California, Berkeley, CA 94720-3840, is published in 10 issues a year. The subscription price for 2019 is US \$635/year for the electronic version, and \$795/year (+\$60, if shipping outside the US) for print and electronic. Subscriptions, requests for back issues, and changes of address should be sent to MSP.

JoMMS peer-review and production is managed by EditFLOW® from Mathematical Sciences Publishers.

PUBLISHED BY

 **mathematical sciences publishers**  
nonprofit scientific publishing

<http://msp.org/>

© 2019 Mathematical Sciences Publishers

<b>Preface</b>	<b>MAURIZIO ANGELILLO and SANTIAGO HUERTA FERNÁNDEZ</b>	<b>601</b>
<b>Studying the dome of Pisa cathedral via a modern reinterpretation of Durand-Claye's method</b>	<b>DANILO AITA, RICCARDO BARSOTTI and STEFANO BENNATI</b>	<b>603</b>
<b>Experimental and numerical study of the dynamic behaviour of masonry circular arches with non-negligible tensile capacity</b>	<b>ALEJANDRA ALBUERNE, ATHANASIOS PAPPAS, MARTIN WILLIAMS and DINA D'AYALA</b>	<b>621</b>
<b>Influence of geometry on seismic capacity of circular buttressed arches</b>	<b>GIUSEPPE BRANDONISIO and ANTONELLO DE LUCA</b>	<b>645</b>
<b>Failure pattern prediction in masonry</b>	<b>GIANMARCO DE FELICE and MARIALaura MALENA</b>	<b>663</b>
<b>Energy based fracture identification in masonry structures: the case study of the church of "Pietà dei Turchini"</b>	<b>ANTONINO IANNUZZO</b>	<b>683</b>
<b>Displacement capacity of masonry structures under horizontal actions via PRD method</b>	<b>ANTONINO IANNUZZO, CARLO OLIVIERI and ANTONIO FORTUNATO</b>	<b>703</b>
<b>Automatic generation of statically admissible stress fields in masonry vaults</b>	<b>ELENA DE CHIARA, CLAUDIA CENNAMO, ANTONIO GESUALDO, ANDREA MONTANINO, CARLO OLIVIERI and ANTONIO FORTUNATO</b>	<b>719</b>
<b>Limit analysis of cloister vaults: the case study of Palazzo Caracciolo di Avellino</b>	<b>ANTONIO GESUALDO, GIUSEPPE BRANDONISIO, ANTONELLO DE LUCA, ANTONINO IANNUZZO, ANDREA MONTANINO and CARLO OLIVIERI</b>	<b>739</b>
<b>The rocking: a resource for the side strength of masonry structures</b>	<b>MARIO COMO</b>	<b>751</b>